Journal of Molecular Catalysis A: Chemical 344 (2011) 28–36

Contents lists available at ScienceDirect

Journal of Molecular Catalysis A: Chemical

journal homepage: www.elsevier.com/locate/molcata

# Evaluation of lanthanide-group promoters on Co–Ni/$Al_2O_3$ catalysts for $CH_4$ dry reforming

Say Yei Foo, Chin Kui Cheng, Tuan-Huy Nguyen, Adesoji A. Adesina*

*Reactor Engineering & Technology Group, School of Chemical Engineering, The University of New South Wales, Sydney, NSW 2052, Australia*

ARTICLE INFO

*Article history:*
Received 15 January 2011
Received in revised form 24 April 2011
Accepted 25 April 2011
Available online 6 May 2011

*Keywords:*
$CO_2$ reforming of $CH_4$
Lanthanide promoter
Cobalt–nickel catalyst
Pauling electronegativity

ABSTRACT

The influence of lanthanide group (Ce, Pr and Sm) promoters on alumina-supported bimetallic Co–Ni catalysts for $CH_4$ dry reforming in a fixed-bed reactor was investigated. Lanthanide doping did not appear to affect $CH_4$ and $CO_2$ consumption rate, however, $H_2$ and CO production rates increased suggesting better utilisation of surface carbonaceous species. Carbon deposition on the promoted catalysts was substantially reduced (by up to 50%), with Ce providing the greatest anti-coking resistance followed by Pr and Sm. The beneficial effects of the promoted catalysts may be attributed to the interaction of the deposited but unconverted $C_xH_{1-x}$ species with the lanthanide oxide in redox reactions, as well as smaller active particle size of the promoted catalysts which was unfavourable for carbon formation. In general, the study shows that attributes (such as product ($H_2$ and CO) formation rate constants and the associated reaction orders as well as the enthalpy and entropy of $CH_4$ adsorption) of the promoted catalysts compared favourably to those of the unpromoted counterpart and are reasonably correlated with the Pauling electronegativity of the dopants. TPR–TPO of used catalysts suggests the presence two types of carbonaceous deposits – a reactive species which is lower in the promoted catalysts, and a relatively unreactive carbon which is present in similar quantities for all the catalysts.



## 1. Introduction

The production of synthesis gas ($H_2$/CO mixture) via dry ($CO_2$) reforming ($CH_4 + CO_2 \rightarrow 2CO + 2H_2$) has attracted significant attention within the past decade due to increased interest in the effective utilisation of $CO_2$ (a greenhouse gas) arising from anthropogenic activities. Indeed, since many gas fields contain copious amounts of $CO_2$, natural gas dry reforming may be readily carried out without pre-separation of $CO_2$ from the natural gas [1] before the latter's conversion to syngas as the feedstock for higher hydrocarbons or clean fuels manufacture (e.g. Fischer–Tropsch synthesis). Additionally, biogas from landfill, sewage sludge digester or anaerobic fermentation contain about 48–65% $CH_4$ and 36–41% $CO_2$ [2], further increasing the attractiveness of dry reforming for its potential as a renewable source of hydrogen and syngas supply [3].

Hydrocarbon reforming is conventionally carried out using supported Ni catalysts due to its high activity and low cost. However they are also susceptible to deactivation by carbon deposition. Noble metals such as Rh, Ru, Pt, Pd and Ir possess activities similar to or higher than Ni catalysts, along with excellent coking resistance [4–6]. However, the use of noble metals is not commercially viable due to limited availability and associated high cost. Therefore, the research on $CH_4$ dry reforming has sought ways to improve Ni-based catalysts, including studies on the effect of supports [7–9], bimetallic catalysts [10,11] and promoters [12–16].

Previous studies in our laboratory as well as by others have shown that bimetallic Co–Ni catalysts offer superior performance for hydrocarbon reforming in terms of activity, stability and synergy compared to monometallic Ni catalyst [11,17]. The use of lanthanide-group metals as catalyst promoters in hydrocarbon reforming is promising, with improved performance in Ce-promoted catalysts attributed to high oxygen storage capacity and hence increased ability to participate in redox reactions with the hydrocarbons [13–15]. Doping of Ni/$Al_2O_3$ with $CeO_2$ has been found to improve Ni reducibility as well as increased metal dispersion, along with suppression of carbon formation due to the oxygen storage capacity of $CeO_2$ [14,15]. The order in which the lanthanide promoters (La and Ce) were added to the catalyst during impregnation did not seem to have any effect on the activity of the doped catalyst [13]. Natesakhawat et al. [15,18] have compared the effect of lanthanide (La, Ce and Yb) promotion in propane steam reforming, and found that doping of Ni/$Al_2O_3$ with 2 wt% rare earth metal results in improved activity, stability and coke resistance, as well as increased Ni reducibility.

In spite of these investigations, there has been no attempt to systematically relate the improvement in these reaction metrics to

* Corresponding author. Tel.: +61 2 9385 5268; fax: +61 2 9385 5966.
*E-mail address:* a.adesina@unsw.edu.au (A.A. Adesina).

1381-1169/$ – see front matter © 2011 Elsevier B.V. All rights reserved.
doi:10.1016/j.molcata.2011.04.018

known indicators of the promoter electronic character. Therefore, in the present study, our aim was to provide empirical correlations between relative performance (dry reforming activity, product $H_2$:CO ratio and carbon deposition rate) of the promoted catalyst to the Pauling electronegativity of the dopants of the Co–Ni catalysts. Specifically, we considered the early members of the lanthanide series, namely: Ce, Pr and Sm.

## 2. Experimental

γ-Alumina (Saint-Gobain Nopro, USA) was first crushed and sieved to 140–425 μm before pre-treatment at 1073 K for 6 h. The promoted catalysts, 2.5L–5Co–15Ni/77.5$Al_2O_3$ (where L = Ce, Pr or Sm, and catalyst composition is in wt%), were prepared via sequential wetness impregnation of metal nitrates (Sigma–Aldrich, Australia) in the order, L, Co and finally Ni. The unpromoted catalyst was prepared similarly, but with the composition 5Co–15Ni/80$Al_2O_3$. Each impregnation step was followed by 3 h of stirring at ambient conditions with subsequent drying for 24 h at 393 K. The resulting dried catalysts were calcined in air at 1073 K for 5 h, at a heating rate of 5 K $min^{-1}$. The calcined catalysts were then crushed and sieved to 140–250 μm before activation in situ in the reactor.

Multipoint BET surface area and pore volume measurements for all catalysts were obtained from $N_2$ adsorption at 77 K on a Quantachrome Autosorb-1 unit. $H_2$-chemisorption, $NH_3$-, $CO_2$- and $CH_4$-temperature-programmed desorption (TPD) were conducted on a Micromeriticx Autochem 2910, in which the catalysts were reduced in situ at 5 K $min^{-1}$ and 1063 K for 2 h prior to each measurement. Pulse $H_2$-chemisorption was conducted at 383 K using 10% $H_2/N_2$ as the pulsing gas and with the sample being degassed under vacuum at 573 K for 3 h before each measurement. $NH_3$, $CO_2$ and $CH_4$ temperature-programmed desorption experiments were performed at heating rates of 10, 15, 20 and 30 K $min^{-1}$, where the probe gases, 10% $NH_3/N_2$. 10% $CO_2$/He and $CH_4$ respectively, were adsorbed at 323 (for $CO_2$) and 423 K (for $NH_3$ and $CH_4$). Powder X-ray diffraction (XRD) analysis was conducted on a Philips X'Pert system using a Ni-filtered Cu Kα radiation (λ = 1.542 Å) at 40 kV and 40 mA. The X-ray diffractograms were analyzed using an X'Pert ScorePlus software. Temperature-programmed reduction (TPR) experiments for fresh catalysts to investigate solid phase changes upon activation, as well as temperature-programmed reduction-oxidation (TPR–TPO) on used catalysts to evaluate carbon removal effectiveness, were conducted on a ThermoCahn TherMax 200 unit. The gaseous products from the temperature-programmed runs were monitored by a Pfeiffer Thermostar quadrupole mass spectrometer. All thermogravimetric experiments were carried out with a gas flow rate of 55 mL $min^{-1}$ (air for oxidation, 50%$H_2$/Ar for reduction) with heating rate of 5 K $min^{-1}$ and holding temperature of 973 K. Total carbon content of used catalysts was determined using a Shimadzu TOC Analyser 5000A coupled to a Solid Sample Module SSM-5000A.

Reaction runs were conducted on a computer-controlled experimental rig consisting of a gas manifold station, a stainless steel fixed-bed reactor (OD = 6.25 mm and ID = 4.57 mm) packed with 0.1 g of catalyst, and a Shimadzu GC-17A gas chromatograph fitted with a thermal conductivity detector and an Alltech CTR-1 column. Prior to each reaction, the calcined catalyst was reduced in situ in 50 mL $min^{-1}$ of 50% $H_2/N_2$ mixture at temperature ramp of 5 K $min^{-1}$, and held at 1063 K for 2 h. Following activation of the catalyst, the reactor was cooled under a blanket of $N_2$ to the reaction temperature. Gas-hourly space velocity of 20,000 $h^{-1}$ and catalyst particles limited to the size range 140–250 μm to minimise transport-disguised kinetics during data analysis. Runs were conducted over the temperature range 923–1023 K, with constant total pressure of 110 kPa. $N_2$ was employed as the diluent gas and tie component for material balance purposes.

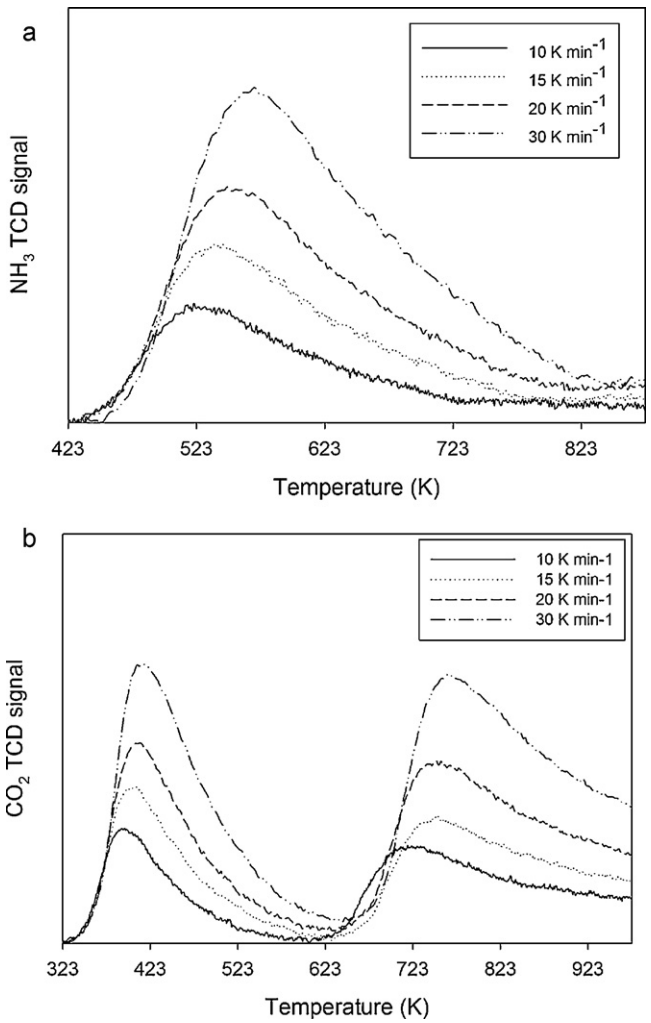


**Fig. 1.** (a) $NH_3$-TPD and (b) $CO_2$-TPD profiles of calcined alumina.

## 3. Results and discussion

### 3.1. Catalyst characterization

Table 1 displays the properties determined from $N_2$ physisorption and $H_2$ chemisorption measurements over the 4 catalysts. Doping with lanthanide did not appear to have any significant effect on the BET surface area, pore volume and pore size of the catalysts. $H_2$ chemisorption results (low metal dispersion, metal surface area and active particle size) were, however, consistent with the high metal loading (≥15 wt%) used. However, there seemed to be a modest increase in metal dispersion and surface area with lanthanide promotion. Increased dispersion of Ce-promoted catalysts has also been reported by Wang and Lu [14] and Nandini et al. [19].

Table 2 summarizes the results obtained from $NH_3$- and $CO_2$-TPD. Fig. 1(a and b) show the $NH_3$-TPD and $CO_2$-TPD profiles for the calcined alumina support while Fig. 2(a and b) depict the same plots for the Ce-promoted catalyst (representative for all four catalysts). TPD experiments were conducted at multiple heating rates

**Table 1**
Physicochemical characteristics of the catalysts.

| | Catalysts | | | | |
|---|---|---|---|---|---|
| | Calcined $Al_2O_3$ support | 5Co–15Ni | 2.5Ce–5Co–15Ni | 2.5Pr–5Co–15Ni | 2.5Sm–5Co–15Ni |
| BET area ($m^2\ g^{-1}$) | 177.0 | 110.8 | 110.7 | 111.3 | 110.4 |
| Pore volume ($cm^3\ g^{-1}$) | 0.794 | 0.496 | 0.454 | 0.483 | 0.436 |
| Average pore size (nm) | 17.93 | 17.91 | 16.38 | 16.38 | 15.90 |
| Metal dispersion (%) | – | 0.580 | 0.653 | 0.655 | 0.591 |
| Metal surface area ($m^2\ g^{-1}$) | – | 0.776 | 0.874 | 0.876 | 0.790 |
| Active particle size (nm) | – | 173.8 | 154.4 | 154.0 | 170.5 |

**Table 2**
Acid–base properties of the catalysts.

| | Peak | Calcined alumina support | 5Co–15Ni | 2.5Ce–5Co–15Ni | 2.5Pr–5Co–15Ni | 2.5Sm–5Co–15Ni |
|---|---|---|---|---|---|---|
| $-\Delta H_{d,\ NH_3}$ ($kJ\ mol^{-1}$) | I | 68.9 | 43.3 | 37.5 | 38.1 | 61.2 |
| | II | – | 71.0 | 71.6 | 70.6 | 86.5 |
| Acid site concentration ($\mu mol\ m^{-2}$) | I | 2.13 | 1.08 | 1.13 | 1.12 | 0.64 |
| | II | – | 2.89 | 2.24 | 2.34 | 2.72 |
| | Total | 2.13 | 3.97 | 3.37 | 3.46 | 3.35 |
| $-\Delta H_{d,\ CO_2}$ ($kJ\ mol^{-1}$) | Ia | 63.2 | 51.3 | 68.5 | 62.1 | 56.2 |
| | Ib | – | 68.0 | 75.2 | 84.6 | 72.5 |
| | II | 68.4 | 73.4 | 86.7 | 45.0 | 45.1 |
| Basic site concentration ($\mu mol\ m^{-2}$) | Ia | 0.14 | 0.202 | 0.242 | 0.216 | 0.174 |
| | Ib | – | 0.21 | 0.28 | 0.22 | 0.21 |
| | II | 0.32 | 1.03 | 0.98 | 0.91 | 0.94 |
| | Total | 0.46 | 1.44 | 1.50 | 1.35 | 1.32 |
| Acid-to-basic site ratio | | 4.63 | 2.75 | 2.24 | 2.56 | 2.53 |

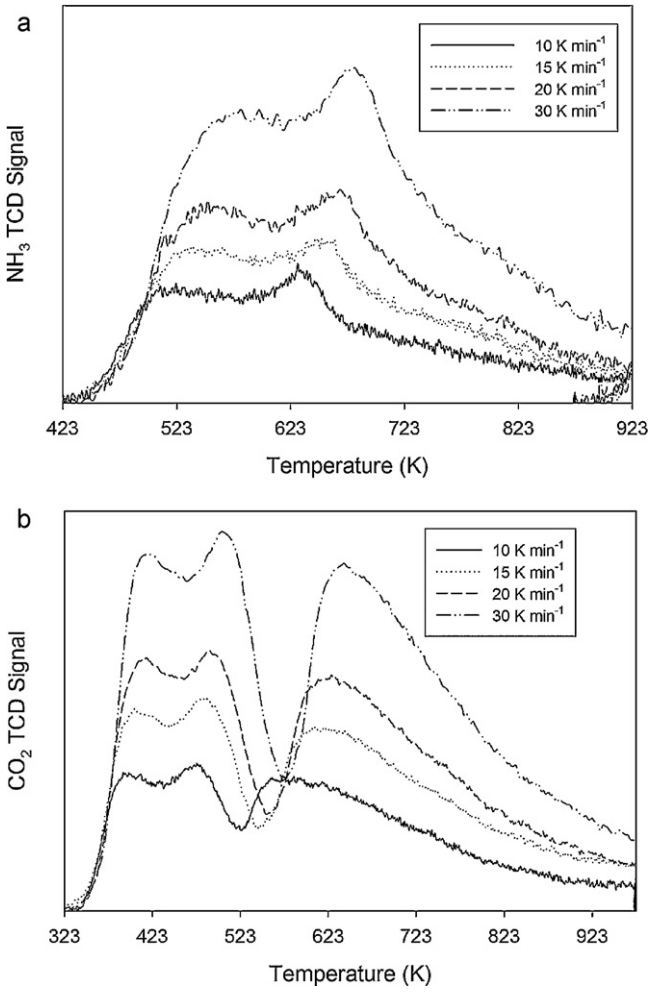


**Fig. 2.** (a) $NH_3$-TPD and (b) $CO_2$-TPD profiles of 2.5Ce–5Co–15Ni.

to determine the heat of desorption, $-\Delta H_d$, using the following general equation:

$$\frac{\ln\ \beta}{T_p^2} = \left(\frac{-\Delta H_d}{R_g T_p}\right) + \ln\left(\frac{-\Delta H_d A_{sat}}{R_g C}\right) \quad (1)$$

where $\beta$ is the temperature ramping rate ($K\ min^{-1}$), $T_p$ is the peak temperature (K), $R_g$ is the gas constant, $A_{sat}$ is the quantity adsorbed at saturation and $C$ is a constant related to desorption rate. $-\Delta H_d$ may be calculated from the slope of a plot of $\ln \beta/T_p^2$ against $1/T_p$. It is evident that the alumina support is characterized by only one peak with a heat of desorption, $-\Delta H_{d,\ NH_3}$ of 68.9 $kJ\ mol^{-1}$, and is identified as a weak Lewis centre from its peak temperature (520–570 K) [20] and also because Brønsted acid sites typically exhibit $-\Delta H_{d,\ NH_3}$ greater than 125 $kJ\ mol^{-1}$ [21]. However, Fig. 1b reveals two types of basic sites. The first peak located at 400–425 K (Ia in Table 2) appeared to be a weak Lewis basic site with a $CO_2$ heat of desorption, $-\Delta H_{d,\ CO_2}$, of 63.2 $kJ\ mol^{-1}$, and a second peak between 720 and 750 K (II in Table 2) was assigned to a Brønsted basic site possibly arising from the presence of surface $OH^-$ species on the alumina [22,23].

$NH_3$-TPD spectra of the catalysts revealed 2 distinct maxima, while $CO_2$-TPD profiles have 3 characteristic peaks as shown in Fig. 2(a and b) respectively. The first $NH_3$-TPD peak is indicative of a weak Lewis acid site which is present on all catalysts and the calcined support – an amphoteric oxide (cf. Fig. 1a), while the second peak (625–700 K) may be attributed to a strong Lewis site [20] probably located at the interface between the metal and the alumina support. Total surface acid site concentration on the promoted catalyst was in general lower than that of unpromoted 5Co–15Ni, but higher than on the pure alumina support (cf. Table 2). The decrease in the acid site concentration for the promoted catalysts is a reflection of the higher electron density introduced by the rare-earth oxides. In the $CO_2$-TPD plot of Fig. 2b, the first peak from Fig. 1b appears to have been bifurcated into two separate peaks (Ia and Ib in Table 2) located at two different temperature windows, namely: 390–425 K and 470–500 K respectively while the peak representing the Brønsted basic site seemed to have shifted to a lower

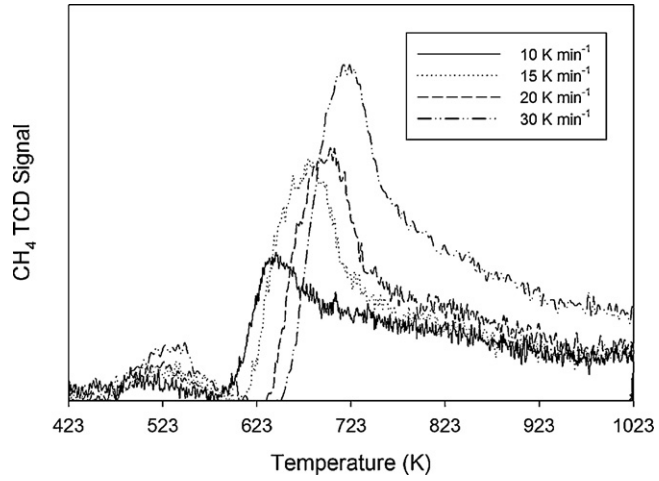


**Fig. 3.** $CH_4$-TPD profile of 2.5Ce–5Co–15Ni.

temperature range (570–640 K). The new intermediate peak, Ib, was categorized as a strong Lewis basic site [22,23]. Although the $CO_2$-TPD data showed that the basic site concentration is practically unaffected by lanthanide promotion, the overall TPD results implicated greater basic characteristics in the lanthanide-doped catalysts, since acid-to-basic site ratios for all promoted catalysts were lower than for the unpromoted catalyst.

The $CH_4$-TPD profile is shown in Fig. 3, where a minor peak between 500 and 540 K and a major peak located in the range 630–725 K suggest two types of sites for $CH_4$ adsorption. The first peak is due to $CH_4$ adsorption on the support since the temperature window is approximately the same as that in the first peak of the $NH_3$-TPD profile of the catalysts (cf. Fig. 2a), while the second peak represents adsorption on the metal (Co/Ni) site on the catalyst. Table 3 summarizes the characteristics of these sites. It is evident from this table that the heat of $CH_4$ adsorption values, $-\Delta H_{d,\,CH_4}$, for the promoted catalysts were higher than that of the undoped catalyst, although the amount of desorbed $CH_4$ was practically the same (ca. 1.1 μmol $m^{-2}$) on all catalysts. Interestingly, the presence of the rare-earth oxides seemed to increase the value of $-\Delta H_{d,\,CH_4}$ for both peaks with a maximum for the Pr-promoted catalyst. In particular, the normalized ratios of the heat of desorption for peaks I and II increased linearly with the Pauling electronegativity [24], χ, as seen in Fig. 4, suggesting that a strong acid site is required for $CH_4$ adsorption.

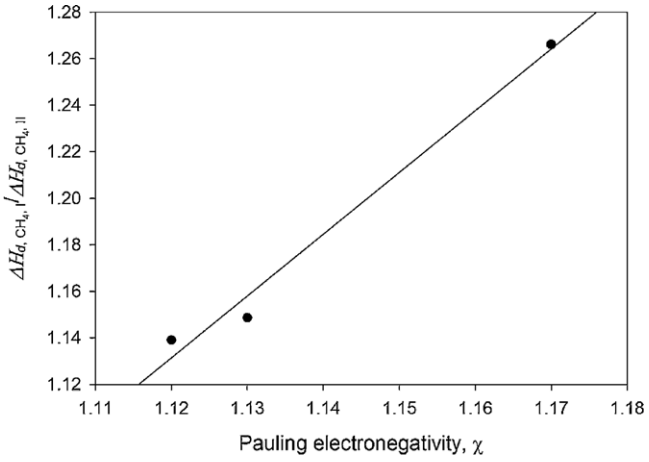


**Fig. 4.** Relationship between $CH_4$ heat of desorption on the promoted catalyst and the corresponding Pauling electronegativity.

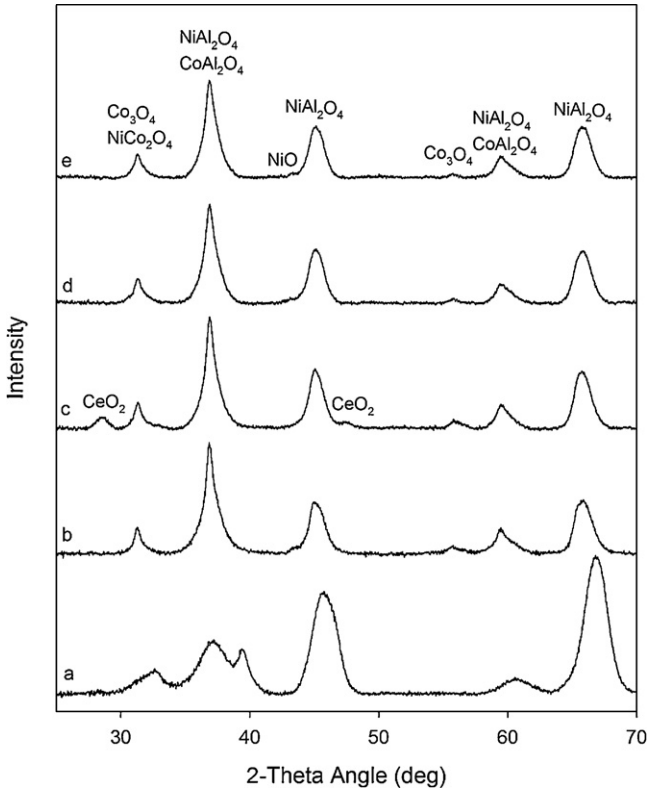


**Fig. 5.** X-ray diffractogram of: (a) γ-$Al_2O_3$, (b) 5Co–15Ni/$Al_2O_3$, (c) 2.5Ce–5Co–15Ni/$Al_2O_3$, (d) 2.5Pr–5Co–15Ni/$Al_2O_3$ and (e) 2.5Sm–5Co–15Ni/$Al_2O_3$.

The formation of metal oxide phases during calcination may be described by:

$$TM(NO_3)_2 \rightarrow TMO + N_2O_5\uparrow; \quad TM = Co \text{ or } Ni \tag{2}$$

$$2L(NO_3)_3 \rightarrow L_2O_3 + 3N_2O_5\uparrow; \quad L = Ce, Pr, Sm \tag{3}$$

$$3CoO + 0.5O_2 \rightarrow Co_3O_4 \tag{4}$$

$$NiO + 2CoO + 0.5O_2 \rightarrow NiCo_2O_4 \tag{5}$$

These phases were confirmed from XRD analysis of the unreduced catalysts as shown in Fig. 5, which indicates the presence of $NiCo_2O_4$ ($2\theta = 31.2^\circ$), $CoAl_2O_4$ ($2\theta = 36.8^\circ$ and $59.1^\circ$), $NiAl_2O_4$ ($2\theta = 36.8^\circ$, $44.8^\circ$, $59.1^\circ$ and $65.7^\circ$) and $Co_3O_4$ ($2\theta = 31.2^\circ$ and $55.3^\circ$) in all catalysts. Additional peaks at $2\theta = 28.4^\circ$ and $47.4^\circ$ representing $CeO_2$ were visible on the Ce-promoted catalyst. However the oxides of Pr and Sm could not be identified from the XRD patterns shown in Fig. 5d and e. The presence of $CeO_2$ phase suggests that the $Ce^{3+}$ precursor was readily oxidised to $Ce^{4+}$ during air calcination as shown by:

$$Ce_2O_3 + 0.5O_2 \rightarrow 2CeO_2 \tag{6}$$

Fig. 6 shows the derivative weight profiles of the catalysts during temperature-programmed reduction. For the unpromoted Co–Ni catalyst, $H_2$-TPR suggests that reduction of $Co_3O_4$ and NiO to CoO and Ni respectively took place at 435 K. $NiCo_2O_4$ was reduced to Ni and CoO at 600 K, while the last two peaks at 740 K and 973 K represent the reduction of CoO to Co and the reduction of the metal aluminates respectively. These TPR peaks were similar to those of Vogelaar et al. [25] and Vos et al. [26] for Ni/$Al_2O_3$, as well as Chu et al. [27] and Cooper et al. [28] for Co/$Al_2O_3$. In particular, at high Ni loadings (>5%), bulk NiO present in small amounts is reduced at a lower temperature than the spinel Ni aluminate phase [25,29], while $Co_3O_4$ was reportedly reduced in a two-step process at similar temperatures [27,28]. The existence of the metal aluminates

**Table 3**
$CH_4$ heat of desorption and amount desorbed during TPD.

| | Peak | 5Co–15Ni | 2.5Ce–5Co–15Ni | 2.5Pr–5Co–15Ni | 2.5Sm–5Co–15Ni |
|---|---|---|---|---|---|
| $-\Delta H_{d,\,CH_4}$ (kJ mol$^{-1}$) | I | 33.8 | 72.2 | 80.0 | 75.5 |
| | II | 29.7 | 55.7 | 61.2 | 52.4 |
| Total amount of $CH_4$ desorbed (μmol m$^{-2}$) | | 1.081 | 1.136 | 1.049 | 1.130 |
| Normalized ratio of $-\Delta H_{d,\,CH_4}$ for peaks I and II | | 1 | 1.14 | 1.15 | 1.27 |
| $\chi$ | | N/A | 1.12 | 1.13 | 1.17 |

**Table 4**
Criteria for absence of transport intrusions in reactor.

| Mass transfer | Heat transfer | | |
|---|---|---|---|
| Criteria | Value | Criteria | Value |
| Mears (external) $(-r_{exp})\rho_b d_p n/0.3k_c C_{A_b} < 1$ | 0.047 | Mears (external) $(\lvert(-\Delta H_r)\rvert(-r_{exp})\rho_b d_p E_A/0.3hT_b^2R) < 1$ | 0.273 |
| Weisz–Prater (internal) $(-r_{exp})\rho_b d_p^2/4D_{eff}C_{A_s} < 1$ | 0.078 | Anderson (internal) $(\lvert(-\Delta H_r)\rvert(-r_{exp})d_p^2\rho_b E_A/3\lambda_{eff}RT_s^2) < 1$ | $3.49 \times 10^{-5}$ |
| Wall effect $d_r/d_p > 10$ | 26.9 | Mears (radial heat effect) $(E_a/RT_w)((\lvert(-\Delta H_r)(-r_{exp})\rho_b[(1-\varepsilon_{bed})/(1-b)d_r^2]/4\lambda_{eff}T_w\rvert)(1/8+1/Bi_w\, d_p/d_r)) < 0.05$ | 0.0052 |

suggests high interaction between the metal and support due to the high calcination temperature used [30]. Catalyst promotion did not seem to alter the major phase changes during reduction. However, reduction peaks for all the promoted catalysts were shifted to lower temperatures by about 50 K (with the exception of the aluminate phase) compared with undoped Co–Ni, suggesting that lanthanide-promotion increased ease of catalyst reduction. Natesakhawat et al. [15] and Gallego et al. [31] have also observed that the TPR peaks of lanthanide-promoted metal catalysts shifted to lower temperatures.

### 3.2. Reaction runs

The reactor operating conditions were chosen to ensure that rate data collected were free from transport intrusions, which were confirmed by the satisfaction of diagnostic criteria as discussed in our previous paper [32] and shown in Table 4. Fig. 7a to d show the reaction rates for $CH_4$, $CO_2$, $H_2$ and CO during $CH_4$ dry reforming at 973 K at varying $P_{CO_2}$ and constant $P_{CH_4}$ (20 kPa). For all catalysts, $CH_4$, $CO_2$ and CO reaction rates experienced an increase with $P_{CO_2}$. On the other hand, the change in $H_2$ production rate with $P_{CO_2}$ was not significant, suggesting that the additional $H_2$ produced from increased $CH_4$ consumption is converted to water via the reverse water-gas shift reaction. $H_2$ production first took place via $CH_4$ dehydrogenation into carbonaceous species, $C_xH_{1-x}$ [32]:

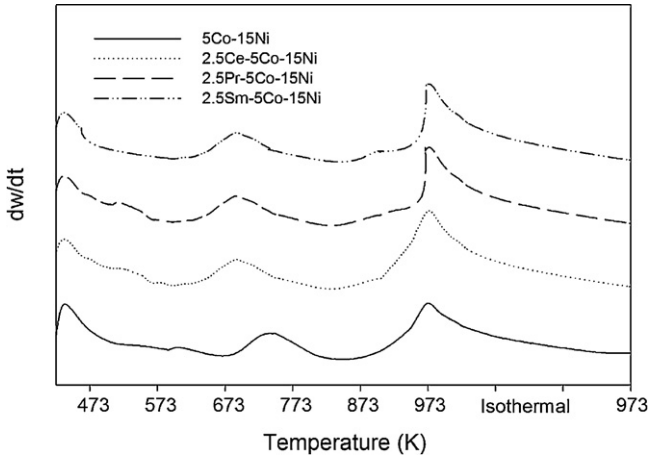


**Fig. 6.** Derivative weight profiles of the catalysts during temperature-programmed reduction.

$$xCH_4 \rightarrow C_xH_{1-x} + \left(\frac{5x-1}{2}\right)H_2 \quad (7)$$

$CO_2$ subsequently reacts with the carbonaceous deposit to yield CO along with further $H_2$ formation via:

$$C_xH_{1-x} + xCO_2 \rightarrow 2xCO + \left(\frac{1-x}{2}\right)H_2 \quad (8)$$

Thus, the combination of Eqs. (7) and (8) gives the overall reaction:

$$CH_4 + CO_2 \rightarrow 2CO + 2H_2 \quad (9)$$

However, the data in Fig. 7a–d indicate that the kinetics of carbon deposition is different from $CO_2$ gasification of the surface carbonaceous species. The apparent lack of change in $H_2$ formation rate under different $P_{CO_2}$ values point to a slower rate for Eq. (8) and hence $(5x-1)$, must be significantly higher than $(1-x)$ or $x$ must be $\geq$0.3. In particular as seen in Fig. 8, for $CO_2$:$CH_4$ < 1, the $H_2$:CO ratio is higher than 1 (greater than stoichiometric expectation) for all catalysts suggesting that the metallic sites ($Co^0$ and $Ni^0$ atoms) were probably converted to surface metal carbides upon $CH_4$ adsorption with concomitant $H_2$ release. However, as the $CO_2$ partial pressure increased, $H_2$:CO decreased from 1 to about 0.6 as the reduced metal sites were most likely re-oxidised in the presence of excess $CO_2$ with attendant high CO partial pressure and hence, the reduced $H_2$:CO ratio observed.

Even so, $CH_4$ and $CO_2$ consumption rates did not seem to vary significantly among the catalysts but $H_2$ and CO production rates were higher in the promoted catalysts. Lanthanides such as Ce are known to possess high oxygen storage capacities [33]. While some surface carbon from Eq. (7) may remain unreacted in the Co–Ni catalyst, additional routes for conversion of $C_xH_{1-x}$ may exist in lanthanide-promoted catalysts via redox reactions:

$$L_\alpha O_\lambda + C_xH_{1-x} \leftrightarrow L_\alpha O_{\lambda-x} + xCO + \left(\frac{1-x}{2}\right)H_2 \quad (10)$$

$$L_\alpha O_{\lambda-x} + xCO_2 \leftrightarrow L_\alpha O_\lambda + xCO \quad (11)$$

where $\alpha$ = 1 or 2; $\lambda$ = 2 or 3; $0.2 < x \leq 1$.

Given that the $H_2$:CO ratio on the promoted catalysts also decreased with increasing $P_{CO_2}$ to below 1 (cf. Fig. 8), the empirical composition of the carbonaceous deposit, $C_xH_{1-x}$, based on Eq. (10) or (11) must be such that $x \geq 0.2$ whereas on the unpromoted catalyst, $x \geq 0.3$ indicating that the carbon layer on the latter would have a lower H:C ratio and therefore more likely to undergo polycondensation to more resistant naphthalenic type species with time

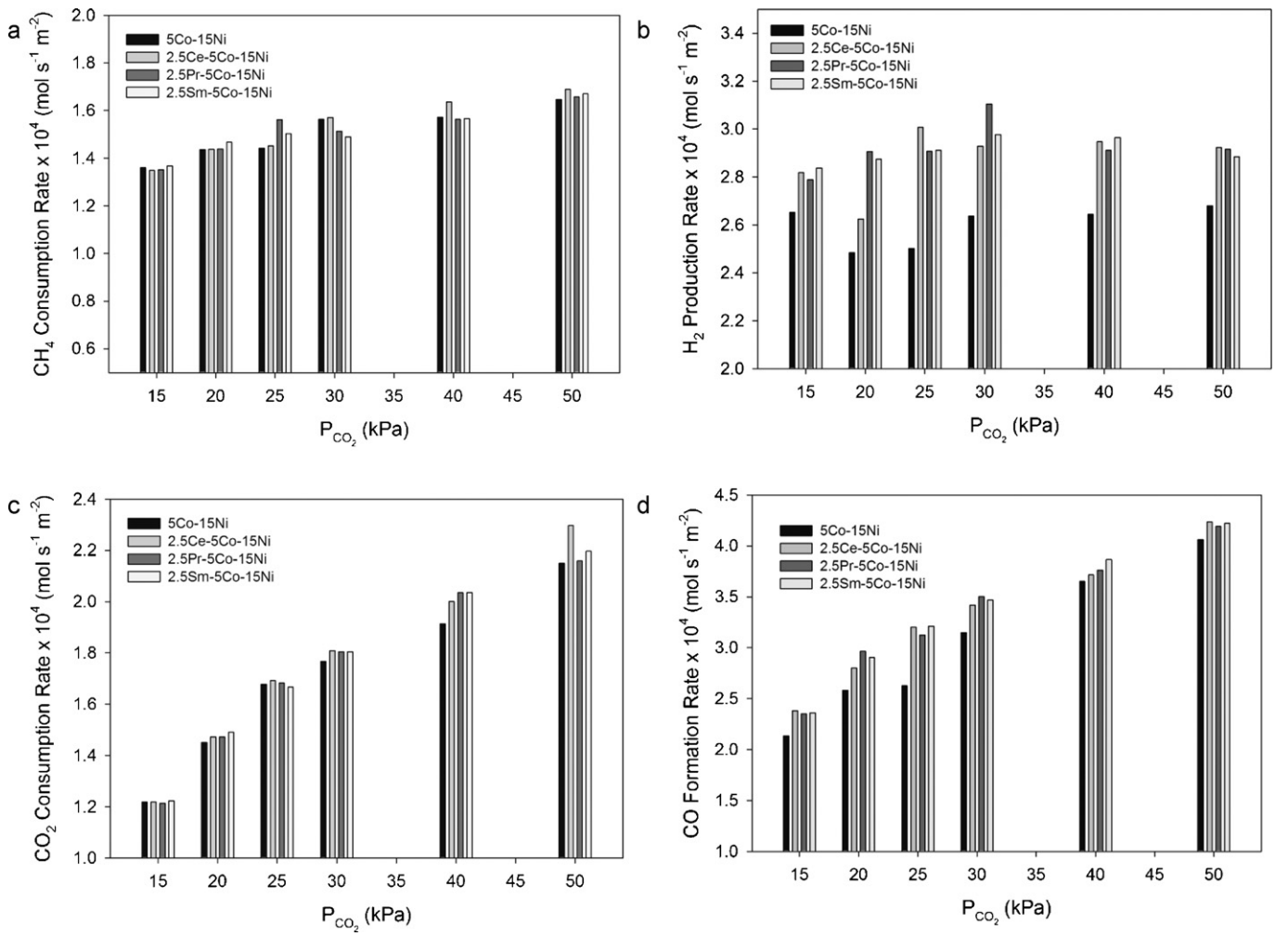


**Fig. 7.** Reaction rates of (a) $CH_4$, (b) $CO_2$, (c) $H_2$ and (d) CO during dry reforming over the various catalysts. Reaction conditions: $P_{CH_4} = 20$ kPa, $T = 973$ K.

on-stream [34]. Thus, lanthanide-promoted hydrocarbon reforming catalysts would exhibit greater coking resilience than the undoped system.

Product $H_2$:CO ratios experienced a nonlinear drop with increased $P_{CO_2}$ for all catalysts, as shown in Fig. 8. In particular, this relationship is captured by the expression [32]:

$$S_{H_2:CO} = \varphi\sigma^{-\gamma} \quad (12)$$

where $\sigma$ is the $CO_2$:$CH_4$ ratio while $\varphi$ represents the ratio of the formation rate constant for $H_2$ to CO and $\gamma$ is the net reaction order with respect to the $CO_2$:$CH_4$ ratio for both $H_2$ and CO. The estimates of these constants for various catalysts are provided in Table 5. Although the $H_2$:CO ratio in $CO_2$-deficient environment (feed $CO_2$:$CH_4 < 1$) is higher in the unpromoted Co–Ni catalyst, this trend was reversed at higher $P_{CO_2}$. Indeed, since stoichiometrically excess $CO_2$ may participate in the additional redox pathways shown in Eq. (10) and (11) in the presence of lanthanide-promoted catalysts, it is likely that the reverse water-gas shift reaction ($CO_2 + H_2 \rightarrow CO + H_2O$) has a greater contribution in the unpromoted catalyst, hence resulting in lower $H_2$ selectivity. Moreover, the parameter estimates from Eq. (12) for the promoted catalysts were normalized ($\varphi_N$ and $\gamma_N$) and correlated with Paul-

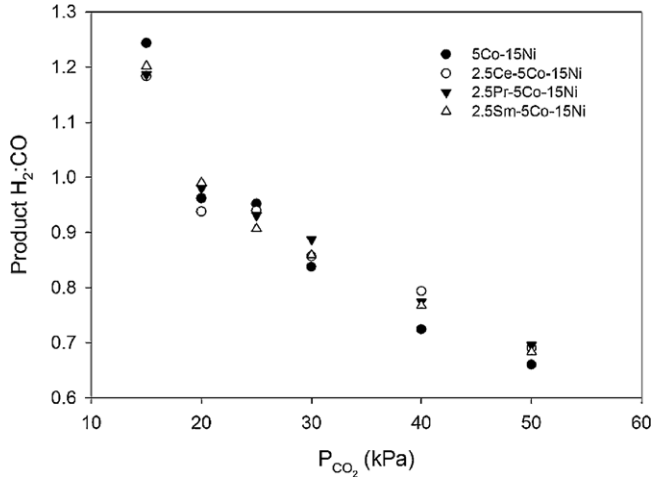


**Fig. 8.** Product $H_2$:CO ratios for dry reforming at 973 K and $P_{CH_4} = 20$ kPa.

**Table 5**
Values of $\varphi$ and $\gamma$, the normalized equivalents (w.r.t. Co–Ni) and Pauling electronegativities [24] of the promoters.

| | 5Co–15Ni | 2.5Ce–5Co–15Ni | 2.5Pr–5Co–15Ni | 2.5Sm–5Co–15Ni |
|---|---|---|---|---|
| $\varphi$ | 4.67 | 3.35 | 3.57 | 3.85 |
| $\gamma$ | 0.50 | 0.40 | 0.42 | 0.44 |
| $\varphi_N$ | 1 | 0.72 | 0.76 | 0.82 |
| $\gamma_N$ | 1 | 0.80 | 0.84 | 0.88 |
| $\chi$ | N/A | 1.12 | 1.13 | 1.17 |

**Table 6**
Summary of kinetic parameter estimates for Langmuir–Hinshelwood model.

| Parameter | 5Co–15Ni | 2.5Ce–5Co–15Ni | 2.5Pr–5Co–15Ni | 2.5Sm–5Co–15Ni |
|---|---|---|---|---|
| $A \times 10^3$ (mol m$^{-2}$ s$^{-1}$ kPa$^{-1}$) | 3.26 | 4.04 | 4.05 | 3.94 |
| $E_a$ (kJ mol$^{-1}$) | 46.7 | 46.9 | 46.9 | 46.6 |
| $\Delta S_{ads,CH_4}$ (J mol$^{-1}$ K$^{-1}$) | −192.7 | −151.4 | −142.4 | −97.1 |
| $\Delta S_{ads,CO_2}$ (J mol$^{-1}$ K$^{-1}$) | −132.1 | −161.3 | −148.9 | −156.5 |
| $\Delta H_{ads,CH_4}$ (kJ mol$^{-1}$) | 131.1 | 173.7 | 181.1 | 221.2 |
| $\Delta H_{ads,CO_2}$ (kJ mol$^{-1}$) | −93.6 | −121.1 | −110.0 | −117.5 |

ing electronegativity, $\chi$ of the rare earth metals [24] as shown in Table 5, thus:

$$\varphi_N = 0.05\ \exp(2.40\chi) \tag{13a}$$

and

$$\gamma_N = 0.12 \exp(1.70\chi) \tag{13b}$$

were obtained with correlation coefficients of 0.94 and 0.97 respectively. These correlations provide a quantitative approach to evaluate the effectiveness of a dopant if the catalytic attributes or performance of the unpromoted catalyst is given.

Given that the same type of sites are present on all four catalysts albeit characterized by different strength and surface density, reaction rate data on each catalyst were individually fitted to the same Langmuir–Hinshelwood kinetic model based on a dual-site mechanism described by the following scheme:

$$CH_4 + 2X_1 \leftrightarrow CH_3\text{-}X_1 + H\text{-}X_1 \tag{14a}$$

$$CH_3\text{-}X_1 + X_1 \leftrightarrow CH_y\text{-}X_1 + H\text{-}X_1\ 1 \le y \le 3$$
$$\vdots \tag{14b}$$
$$CH\text{-}X_1 + X_1 \leftrightarrow C\text{-}X_1 + H\text{-}X_1$$

$$CO_2 + 2X_2 \leftrightarrow CO\text{-}X_2 + O\text{-}X_2 \tag{14c}$$

$$C\text{-}X_1 + O\text{-}X_2 \rightarrow CO\text{-}X_2 + X_1 \quad \text{r.d.s.} \tag{14d}$$

$$2H\text{-}X_1 \leftrightarrow H_2 + 2X_1 \tag{14e}$$

$$CO\text{-}X_2 \leftrightarrow CO + X_2 \tag{14f}$$

$$H\text{-}X_1 + O\text{-}X_2 \rightarrow OH\text{-}X_2 + X_1 \tag{14g}$$

$$H\text{-}X_1 + OH\text{-}X_2 \leftrightarrow H_2O + X_1 + X_2 \tag{14h}$$

where $X_1$ (strong Lewis acid site) and $X_2$ (Brønsted basic site) are two different active sites. Eq. (14d) represents the rate-determining step, while the reaction rate is expressed by:

$$-r_{CH_4} = \frac{k_{rxn}\sqrt{P_{CH_4}}\sqrt{P_{CO_2}}}{(1+\sqrt{K_{CH_4}P_{CH_4}})(1+\sqrt{K_{CO_2}P_{CO_2}})} \tag{15}$$

where the kinetic parameters $k_{rxn}$, $K_{CH_4}$ and $K_{CO_2}$ are described by Eq. (16a) to (16c), and the values of these parameter estimates are given in Table 6. Additionally, the parity plot of Fig. 9 demonstrated a good fit of the data with predicted values

$$k_{rxn} = A\ \exp\left(\frac{-E_a}{RT}\right) \tag{16a}$$

$$K_{CH_4} = \exp\left(\frac{\Delta S_{ads,CH_4}}{R}\right)\exp\left(\frac{-\Delta H_{ads,CH_4}}{RT}\right) \tag{16b}$$

$$K_{CO_2} = \exp\left(\frac{\Delta S_{ads,CO_2}}{R}\right)\exp\left(\frac{-\Delta H_{ads,CO_2}}{RT}\right) \tag{16c}$$

It is apparent from Table 6 that the activation energy, $E_a$, is practically invariant with promoter addition and type. However, both the entropy and enthalpy of $CH_4$ adsorption display a dependency on catalyst type. Specifically, the normalized values of $\Delta S_{ads,CH_4}$ and $\Delta H_{ads,CH_4}$ with respect to the unpromoted catalyst show linear relationships to Pauling electronegativity, $\chi$, given by:

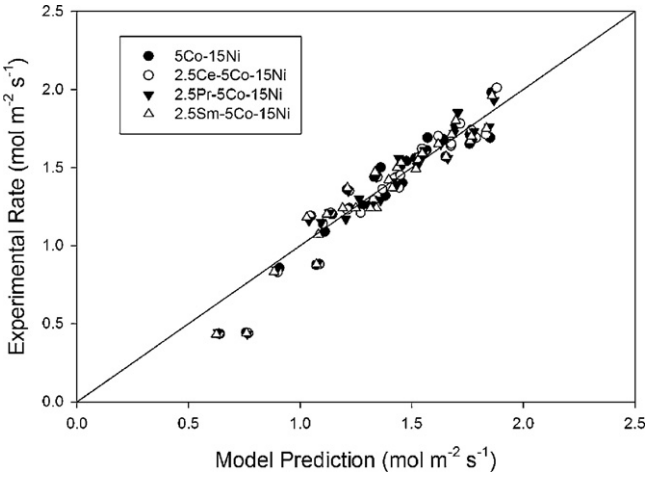


**Fig. 9.** Parity plot comparing experimental rates with values predicted by model.

$$(\Delta S_{ads,CH_4})_{\text{normalized}} = 7.18 - 5.71\chi \tag{17a}$$

and

$$(\Delta H_{ads,CH_4})_{\text{normalized}} = 7.36\chi - 6.93 \tag{17b}$$

with correlation coefficients greater than 0.99, where $(\Delta J_{ads,CH_4})_{\text{normalized}} = ((\Delta J_{ads,CH_4})_{\text{promoted}}/(\Delta J_{ads,CH_4})_{\text{unpromoted}})$, and $J$ is the thermodynamic variable $H$ or $S$. On the other hand, similar estimates for $CO_2$ adsorption do not show a discernible pattern with respect to variation in Pauling electronegativity. This is consistent with the proposition of $CO_2$ adsorption on a Brønsted basic site ($X_2$) found only on the support. Furthermore, the heat of adsorption for $CO_2$ on all four catalysts is exothermic as may

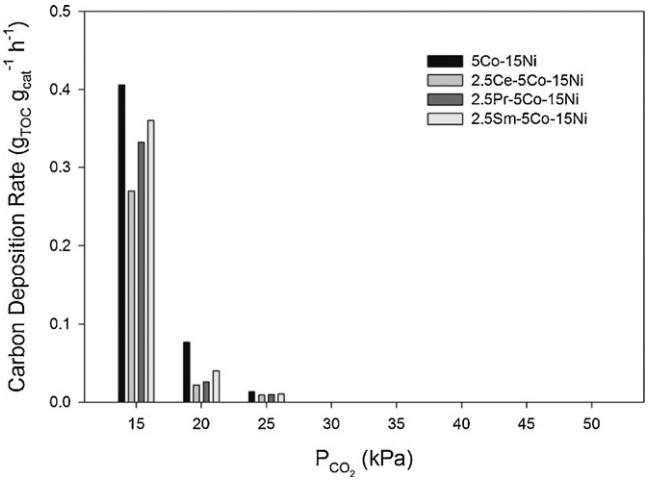


**Fig. 10.** Carbon deposition rate at various $P_{CO_2}$, $P_{CH_4}$ = 20 kPa, $T$ = 973 K.

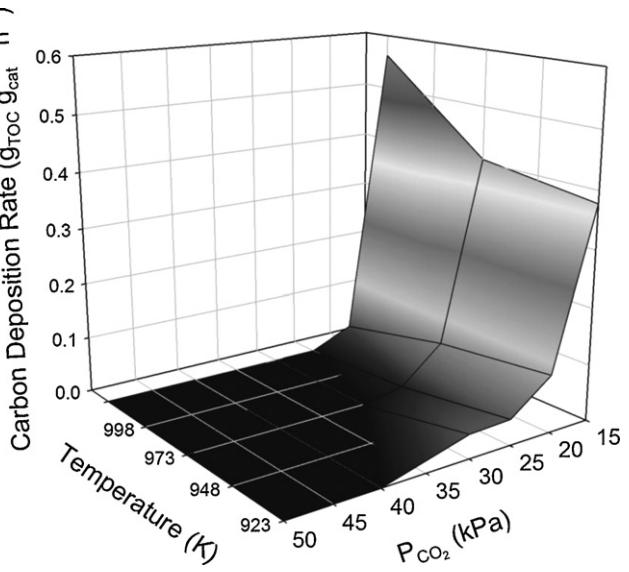


**Fig. 11.** Carbon deposition rate on 5Co–15Ni over varying $P_{CO_2}$ and $T$ at $P_{CH_4}$ = 20 kPa.

be expected for the acid-base reaction ($OH^-_{ads} + CO_2 \rightarrow HCO_{3,ads}^-$) whereas the adsorption of $CH_4$ on $X_1$ (strong Lewis acid site) is endothermic across all catalysts. The lack of a distinct trend on the adsorption equilibrium parameters associated with $X_2$ is due to the diffused effect of the electronic character of the rare-earth oxide on the alumina support whereas there is a more predictable pattern for its influence on $X_1$ located in the Co/Ni oxide phase.

### 3.3. Carbon deposition

Fig. 10 shows the carbon deposition rate on the 4 catalysts during $CH_4$ dry reforming as a function of $P_{CO_2}$ at 973 K. Clearly, lanthanide promotion results in greater resistance to carbon deposition, due to the occurrence of redox reactions (cf. Eqs. (10) and (11)) in the promoted catalysts. The smaller active particle size of the promoted catalysts also probably contributed to increased carbon resistance, since the metal particle size required for carbon formation is larger than that required for $CH_4$ reforming [35]. The bar plot also reveals the superiority of Ce over Pr and Sm in providing coking resistance (Ce > Pr > Sm). The superiority of Ce over the other two lanthanides is possibly due to the electronic properties of the promoters. Unlike Pr and Sm, Ce also possess higher energy 5d electrons which may allow it to interact more readily with carbon. The existence of the higher energy 5d electron in Ce is also reflected in its slightly lower electronegativity compared with Pr and Sm.

The 3D plot (carbon deposition rate-temperature $P_{CO_2}$ behaviour) for the unpromoted Co–Ni is displayed in Fig. 11, and it is representative of the pattern for all the 4 catalysts studied. It is evident that in a $CO_2$-deficient environment, carbon deposition increased with temperature. However, at $CO_2$:$CH_4$ ≥1, the degree of carbon deposition showed a reciprocal relationship with temperature. This carbon deposition rate behaviour may be explained in Fig. 12, where it can be seen that $CO_2$ gasification of carbon becomes thermodynamically more feasible at higher temperatures compared with $CH_4$ dehydrogenation.

Fig. 13 shows the reaction products as detected by mass spectrometry during TPR–TPO of the used catalyst (obtained after 4 h with stoichiometric dry reforming at 923 K). In the TPR stage, $CH_4$ was produced from the reaction between surface $C_xH_{1-x}$ species with $H_2$, and there was no detectable $C_{2+}$ products (cf. Fig. 13a). Nevertheless, the surface carbon layer that was resistant to removal with hydrogen in the TPR stage, was fully oxidised to $CO_2$ during the TPO regime as shown by Fig. 13b with no other products formed. It may be seen that $CH_4$ production profile during TPR stage was characterized by a sharp peak followed by gentle decline during TPR, suggesting the presence of two types of carbonaceous species – one which is easily gasified by hydrogen and another which can only be completely removed by oxygen. Lanthanide promotion resulted in decreased $CH_4$ production during the TPR stage, with $CO_2$ production during TPO relatively unaffected. This suggests that the carbon species which participate in the redox reactions with the rare-earth oxides are of the more reactive nature.

## 4. Conclusions

The beneficial effects of doping Co–Ni dry reforming catalysts with lanthanides have been investigated. Although $CH_4$ and $CO_2$ consumption rates did not seem to be affected by lanthanide promotion, redox reactions between surface $C_xH_{1-x}$ and lanthanide oxides resulted in higher $H_2$ and CO production rates as well as greater carbon resistance in the promoted catalysts, with the degree of coking resistance of the promoters in the order: Ce > Pr > Sm. Decreased metal particle size also contributed to the

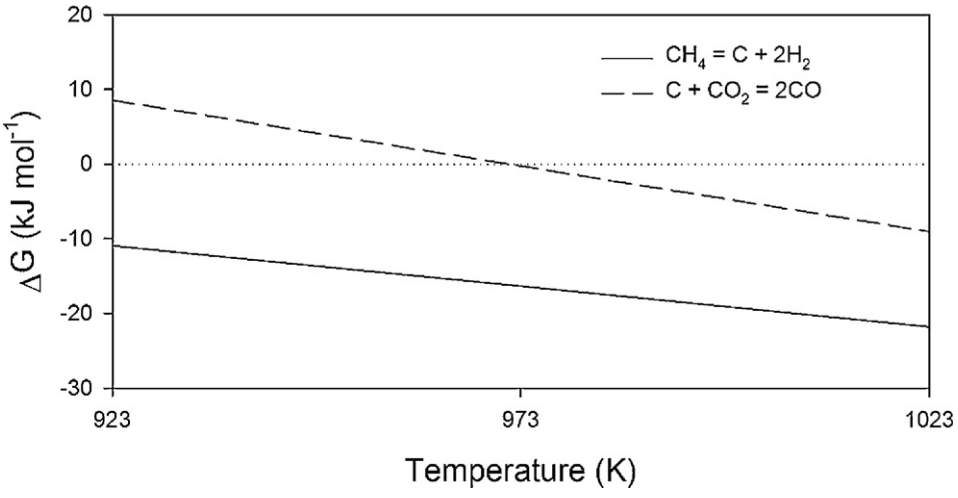


**Fig. 12.** Change in Gibbs free energy with temperature, for $CH_4$ decomposition and $CO_2$ gasification of carbon reactions.

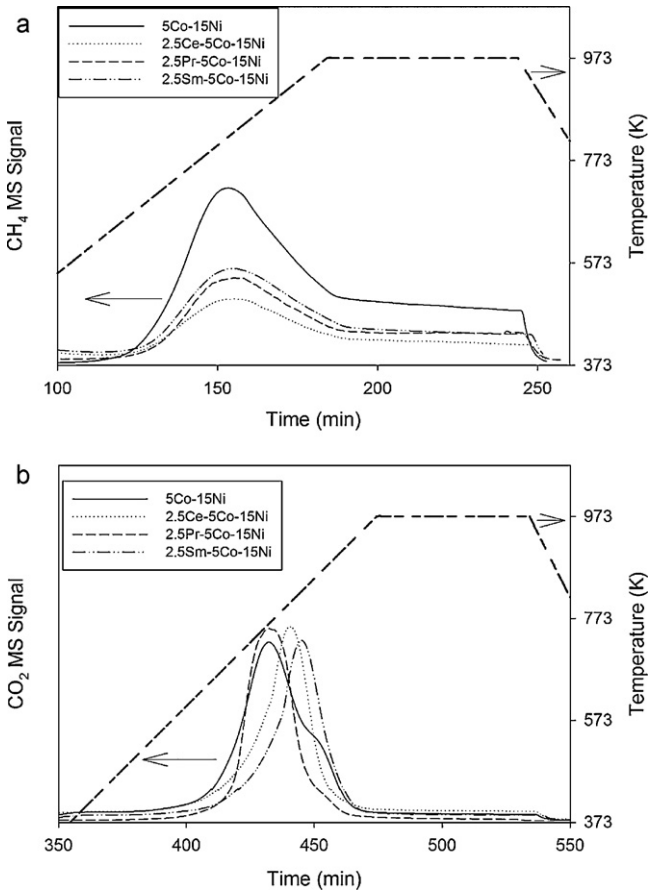


**Fig. 13.** Reaction products as detected by mass spectrometry during TPR–TPO of used 5Co–15Ni catalyst after 4 h reaction run ($P_{CH_4} = P_{CO_2} = 20$ kPa, $T = 923$ K): (a) $CH_4$ produced during TPR and (b) $CO_2$ produced during TPO.

anti-coking ability of the promoted catalysts. The $CH_4$ heat of adsorption, product formation rate constant and reaction orders of the promoted catalysts compared well to those of the unpromoted counterpart, and are reasonably correlated with the Pauling electronegativity of the dopants. While this inference is based only on the examination of three rare-earth metals with relatively close Pauling electronegativity values, the present treatment may serve as a stimulus for a more comprehensive quantitative approach to the prediction of the catalytic behaviour of promoted catalysts if the performance of the unpromoted counterpart is known given that many catalytic phenomena are explained via the electronic theory of catalysis in conjunction with and complementary to, the geometric approach. Additionally, in the present study, TPR–TPO of the used catalysts suggests the presence of two carbonaceous pools – one which is easily gasified by hydrogen and another which may only be removed completely by oxygen. Lanthanide promotion reduces the amount of reactive carbon deposits, but is unable to remove the unreactive species.

## Acknowledgements

The authors acknowledge support from the Australian Research Council. SYF and CKC are recipients of the Australian Postgraduate Award and University International Postgraduate Award scholarships respectively.

## References

[1] Y.H. Hu, E. Ruckenstein, Adv. Catal. 48 (2004) 297.
[2] S. Rasi, A. Veijanen, J. Rintala, Energy 32 (2007) 1375.
[3] C.S. Lau, A. Tsolakis, M.L. Wyszynski, Int. J. Hydrogen Energy 36 (2011) 397.
[4] A.T. Ashcroft, A.K. Cheetham, M.L.H. Green, P.D.F. Vernon, Nature 352 (1991) 255.
[5] M. García-Diéguez, I.S. Piesta, M.C. Herrera, M.A. Larrubia, L.J. Alemany, J. Catal. 270 (2010) 136.
[6] Z. Hou, P. Chen, H. Fang, X. Zheng, T. Yashima, Int. J. Hydrogen Energy 31 (2006) 555.
[7] L.B. Råberg, M.B. Jensen, U. Olsbye, C. Daniel, S. Haag, C. Mirodatos, A.O. Sjåstad, J. Catal. 249 (2007) 250.
[8] E. Ruckenstein, Y.H. Hu, J. Catal. 162 (1996) 230.
[9] S. Wang, G.Q. Lu, Appl. Catal. B 16 (1998) 269.
[10] K. Takanabe, K. Nagaoka, K. Nariai, K. Aika, J. Catal. 232 (2005) 268.
[11] J. Zhang, H. Wang, A.K. Dalai, J. Catal. 249 (2007) 300.
[12] T. Horiuchi, K. Sakuma, T. Fukui, Y. Kubo, T. Osaki, T. Mori, Appl. Catal. A 144 (1996) 111.
[13] Z. Cheng, Q. Wu, J. Li, Q. Zhu, Catal. Today 30 (1996) 147.
[14] S. Wang, G.Q. Lu, Appl. Catal. B 19 (1998) 267.
[15] S. Natesakhawat, O. Oktar, U.S. Ozkan, J. Mol. Catal. A: Chem. 241 (2005) 133.
[16] R. Martinez, E. Romero, C. Guimon, R. Bilbao, Appl. Catal. A 274 (2004) 139.
[17] K. Opoku-Gyamfi, K. Tafreshi, A.A. Adesina, React. Kinet. Catal. Lett. 64 (1998) 229.
[18] S. Natesakhawat, R.B. Watson, X. Wang, U.S. Ozkan, J. Catal. 234 (2005) 496.
[19] A. Nandini, K.K. Pant, S.C. Dhingra, Appl. Catal. A 290 (2005) 166.
[20] R. Barthos, F. Lønyi, G. Onyestyák, J. Valyon, Solid State Ionics 141–142 (2001) 253.
[21] G. Yaluris, R.B. Larson, J.M. Kobe, M.R. González, K.B. Fogash, J.A. Dumesic, J. Catal. 158 (1996) 336.
[22] T. López, R. Gómez, M.E. Llanos, E. García-Figueroa, J. Navarrete, E. López-Salinas, Mater. Lett. 39 (1999) 51.
[23] A.V. Salker, S.J. Naik, Appl. Catal. B 89 (2009) 246.
[24] A.L. Allred, J. Inorg. Nucl. Chem. 17 (1961) 215.
[25] B.M. Vogelaar, A.D. van Langeveld, P.J. Kooyman, C.M. Lok, R.L.C. Bonné, J.A. Moulijn, Catal. Today (2010), doi:10.1016/j.cattod.2009.11.018.
[26] B. Vos, E. Poels, A. Bliek, J. Catal. 198 (2001) 77.
[27] W. Chu, P.A. Chernavskii, L. Gengembre, G.A. Pankina, P. Fongarland, A.Y. Khodakov, J. Catal. 252 (2007) 215.
[28] C.G. Cooper, T.H. Nguyen, Y.J. Lee, K.M. Hardiman, T. Safinski, F.P. Lucien, A.A. Adesina, Catal. Today 131 (2008) 255.
[29] C. Li, Y.W. Chen, Thermochim. Acta 256 (1995) 457.
[30] K.M. Hardiman, C.G. Cooper, A.A. Adesina, Ind. Eng. Chem. Res. 43 (2004) 6006.
[31] G.S. Gallego, J.G. Marín, C. Batiot-Dupeyrat, J. Barrault, F. Mondragón, Appl. Catal. A 369 (2009) 97.
[32] S.Y. Foo, C.K. Cheng, T.H. Nguyen, A.A. Adesina, Ind. Eng. Chem. Res. 49 (2010) 10450.
[33] K. Otsuka, T. Ushiyama, I. Yamanaka, Chem. Lett. 22 (1993) 1517.
[34] K.M. Hardiman, T.T. Ying, A.A. Adesina, E.M. Kennedy, B.Z. Dlugogorski, Chem. Eng. J. 102 (2004) 119.
[35] J.R. Rostrup-Nielsen, H.B. Calvin, B.B. John, Stud. Surf. Sci. Catal. 68 (1991) 85.